SSRG International Journal of Electrical and Electronics Engineering
ISSN: 2348-8379/ https://doi.org/10.14445/23488379/IJEEE-V11I6P131

Volume 11 Issue 6, 305-316, June 2024

Original Article

Smart Flow Management for Hybrid PV-Wind Connected Water Pumping Systems: Optimized UPFC and Fuzzy Q-Learning Control

P. Nagendra[1], K. Sasikala[2]

[1,2]*Department of EEE, School of Engineering, Vels Institute of Science Technology & Advanced Studies, Tamilnadu, India.*

[1]*Corresponding Author : pathakotlanagendra@gmail.com*

Received: 14 April 2024 Revised: 17 May 2024 Accepted: 14 June 2024 Published: 29 June 2024

Abstract - *Remote areas need to prioritize the pumping of water for agricultural and drinking purposes. Water pumping is a promising and advantageous application of renewable energy sources, such as hybrid energy sources that combine photovoltaic and wind power. A novel approach to effective flow control in hybrid PV and wind-powered water pumping systems is presented in this research. To optimize a Proportional Integral Derivative (PID) controller that governs motor speed, the proposed approach combines an optimized control algorithm, Unified Power Flow Controller (UPFC), and Fuzzy Q-learning. The main goal is to use UPFC to identify and mitigate Power Quality (PQ) issues. To achieve optimal UPFC operation under a range of solar and wind energy conditions, the Kookaburra Optimization Algorithm (KOA) is utilized. Fuzzy Q-learning provides adaptive parameter tuning based on real-time feedback and system dynamics, enabling the PID controller to be tuned online. Moreover, the detailed models of wind and photovoltaic systems highlight their influence on water pumping technology. A PID controller controlled by the KOA algorithm powers the UPFC, a crucial part of the system. The KOA is applied to optimize PID parameters for the UPFC, resulting in a unique contribution that emulates the hunting behavior of kookaburras for both local and global exploration. The PID controller can be easily adjusted online by the Fuzzy Q-Learning algorithm, which improves system stability when reacting to changing energy and environmental conditions. The combination of the Kookaburra Optimization Algorithm, PID control, and UPFC offers a sophisticated and flexible approach to the best possible operation of water pumping systems. Total Harmonic Distortion (THD) is successfully decreased by the proposed method, indicating better waveform quality and fewer harmonic components in the electrical system. The system's ability to maintain a high-quality power supply is reflected in the THD value of 3.92% at 50Hz.*

Keywords - *Water pumping systems, Unified Power Flow Controller (UPFC), Kookaburra Optimization Algorithm (KOA), PID controller and Fuzzy Q-learning.*

1. Introduction

Reducing the impact of generating energy on carbon dioxide emissions is believed to be possible through the utilization of renewable energy. Among these alternative energy sources, solar energy stands out because it provides a number of advantages, such as being environmentally friendly, requiring little maintenance, and having no fuel costs [1]. The highest producing level among the renewable energy sources currently in use is Photovoltaic (PV).

Over the previous five years, solar energy was expected to account for nearly 60% of newly installed clean energy capacity [2]. It is anticipated that by 2025, 27 percent of the world's electricity will come from solar energy. Water supply for remote and rural areas can be achieved through the use of photovoltaic water pumping systems, a widely adopted and promising application of photovoltaic systems [3]. Solar water pumping systems became more viable, and solar panel prices decreased as photovoltaic technology advanced [4]. This kind of water pumping system has certain disadvantages, like low conversion efficiency and temperature fluctuations. Power from the wind has been utilized for water pumping applications. The fluctuating wind speed during the day and the noise generated by the spinning of the wind turbines are two drawbacks of utilizing wind power systems [5].

Applications include drainage, irrigation, cattle watering, salt pans, and residential and communal water supply. Reducing reliance on fossil fuels can be achieved in large part by combining solar and wind energy [6]. Apart from facilitating distributed generation in areas lacking large-scale power generation, it also offers advantages in terms of increased efficiency and dependability. Examples of small-scale power generation include individual photovoltaic cells

and micro wind turbines [7]. A hybrid wind/Photovoltaic (PV) system improves available energy capture, boosts system reliability, and requires less maintenance [8]. Hybrid energy systems have been shown to have a significant impact on lowering reliance on fossil fuels and providing environmentally friendly energy to isolated rural areas for purposes such as water pumping and electrification. As a result, they aid in the mitigation of greenhouse gas emissions [9].

A major concern is the potential improvement of the system's performance and dependability through combining solar and wind energy resources. Numerous studies focus on maximizing power harvested from PV systems through Maximum Power Point Tracking (MPPT) techniques at any operating point, as well as motor efficiency maximization [10]. Such methods operate under the assumption that the DC output voltage will be driven to the maximum power value by means of a DC-DC converter. Many tracking control schemes for PV system MPPT were demonstrated [11]. These methods mostly involve controlling the converters' duty cycle to compel the photovoltaic cell to run at its peak power. Incremental conductance (INC), Constant voltage (CV) and Perturb and observe (P and O) are the most widely used systems in commercial DC-DC converters [12].

Optimizing performance and energy utilization in a hybrid system requires effective power flow management. In order to balance and distribute power between PV and wind sources based on demand and conditions in real time, smart flow management strategies employ sophisticated control techniques [13]. An important component in regulating power flow within the electrical grid is the UPFC. Researchers seek to improve the stability, dependability, and overall efficiency of hybrid PV-wind water pumping systems by optimizing UPFC parameters [14].

This research uses the Unified Power Flow Controller (UPFC) and a new hybrid optimization algorithm to address Power Quality (PQ) problems in hybrid PV-wind connected water pumping systems. The main goal is to effectively identify and address PQ problems so that the water pumping system runs smoothly and dependably. This research's main component is the application of UPFC, a versatile device with controllable voltage, impedance, and power flow. To improve its effectiveness in reducing PQ problems in the hybrid system, the study indicates an optimized UPFC configuration.

In addition, a Fuzzy Logic Controller (FLC) is introduced to improve the control strategy even more. To enhance the adaptability and learning capabilities of the FLC, an innovative approach is introduced: Fuzzy Q-Learning Control [15]. The system's response to varied operating conditions provides the controller with the opportunity to continuously learn from and enhance its decision-making process due to the reinforcement learning technique. The goal of integrating Q-learning is to optimize the control strategy and guarantee effective, real-time power flow management in the hybrid system. The major contributions of this work are,

- The hybrid system has benefited greatly from the addition of UPFC. The UPFC is used to detect and address Power Quality (PQ) problems, improving the water pumping system's overall dependability and performance.
- A creative addition is the use of the Kookaburra Optimization Algorithm for UPFC parameter optimization.
- Fuzzy Q-Learning integration offers adaptive parameter tuning based on system dynamics and real-time feedback. As a result, system stability can be improved in response to shifting energy and environmental conditions by tuning the PID controller online.

The structure of the paper is as follows: Section 2 represents a review of the relevant literature. Section 3 delves into the proposed method, and Section 4 discusses the obtained results. Finally, Section 5 concludes the paper.

2. Literature Review

Numerous related works have been explored in this section related to water pumping systems. Altimania et al. (2023) [16] have suggested innovatively using a three-phase induction motor to increase the daily volume of water pumped using a photovoltaic system. The strategy took into account increasing the power collected from the PV system as well as the three-phase induction motor's efficiency. The PV system's MPPT enabled the harvesting. The method was used at any operating point on a PV-powered three-phase Induction Motor Water Pumping System (PV-IMWPS).To achieve MPPT for the PV system, maximize pump flow rate, and guarantee maximum motor effectiveness at all temperatures and irradiances, this flux control was suggested.

Carricondo-Antón et al. (2023) [17] have examined a particular instance of a standalone solar system intended to pump water. In order to meet the requirements for pumping water and reduce overall installation costs, they divided the required total pump power among several smaller pumps in the required PV generator. The variability of solar radiation was taken into account when dimensioning photovoltaic pumping systems to maximize the amount of energy that could be generated, particularly during low-light conditions. Through a case study analysis, the study investigated the effects of expanding the number of parallel pumps while keeping the overall power and the association between the power of the pumping system and the installed photovoltaic capacity to meet pumping requirements all year long.

De Oliveira Ferreira et al., (2020) [18] have suggested, created a computational model, and examined a hybrid PV-wind water pumping system. The Multi-Input DC-DC Converter (MIC) in the suggested system connected the

energy sources, and its output was connected straight to a DC motor pump without the need for a battery. To operate the sources at specific points on their characteristic curves, the MIC operated either simultaneously or independently on their drained currents.

Alqahtani et al. (2023) [19] have explored the construction and assessment of an energy storage system using pumped hydropower that is linked to a hybrid system comprising wind turbines and solar panels. The idea of the analysis was to assess the ability and efficiency of combining pumped hydro storage with these renewable energy sources. The research findings shed light on this integrated system's potential to improve energy storage and utilization in the production of sustainable power.

Ben Rhouma et al. (2023) [20] have concentrated on a hybrid (PV–Wind) generator that supplies a WPS. Centrifugal pumps powered by variable-speed Induction Motors (IM) under Field-Oriented Control (FOC) were used in the water pumping system. The primary advancement in the contribution was the standardization of the FOC strategy to separate sources and power demand, coupled with the lack of battery storage. Additionally, the lack of battery storage forced the system to stabilize at a steady state, which was required by the hydraulic load characteristics as well as the sporadic renewable energy sources.

Li et al. (2020) [21] have examined the optimization of a hybrid generation WPS in isolated agricultural areas with low electrical power using PV panels, a wind generator, and batteries. The goal was to diminish the annual cost by establishing a universal size optimization model that would identify the best system configuration based on local crop irrigation schedules and climate conditions. The model considered constraints such as battery state of charge and electrical supply reliability. The best setup for greenhouse-growing tomatoes was found by applying the Particle Swarm Optimization (PSO) algorithm.

Bakır et al. (2023) [22] have examined the modelling and optimization control of a hybrid WPS that includes a PV array, battery storage, and a brushless DC motor. External power sources could be avoided by using the PV array to replenish the battery when the water supply was not required. A control system that used a bidirectional converter and loops to regulate DC voltage and battery power was included. The performance of the water cycle algorithm was contrastedto alternative approaches based on settling time and overshoot values. The algorithm modified control parameters to minimize tracking errors.

Menesy et al. (2023) [23] have investigated the most effective layout for a stand-alone hybrid Renewable Energy System (RES) that includes energy storage such as a hydro-pumped storage system, PV, biomass, and Wind Turbine (WT)sources. The issue of determining the ideal size for the generating units in the suggested energy system was approached as an optimization problem, and to determine the ideal size for each part of the suggested grid-independent hybrid system, various algorithms were used, including Heap Based Optimizer (HBO), Grey Wolf Optimizer (GWO), and PSO.

Priyadarshi et al. (2020) [24] have provided experimental validation of the functionality of a modified Artificial Bee Colony (ABC) based MPPT system for a PV Wind HRE system intended for an induction centrifugal pump application fed by a CUK converter through the use of the dSPACE real-time interface. To determine the tuned parameters of a PI Controller, PSO-based evolutionary algorithms were used. For improved DC link utilization and low output THD, the SVPWM-based inverter was modified. For the induction centrifugal pump used in home and agricultural irrigation, traditional V/f control schemes were used to regulate the induction motor's speed.

Stoyanov et al. (2021) [25] have offered a sizing methodology for a hybrid system with water tank storage, wind, and PV based on the assessment of the entire conversion of the energy chain using energy simulations and a one-year operation simulation. A piecewise interpolation was utilized to model the wind generator, and a reduced Durisch's model was used to model the PV generator. Specific crops and meteorological data from sites in Bulgaria were used to apply the methodology. Combinations of water tank capacities and wind (various types) and Photovoltaic (PV) generators were taken into consideration and discussed. Three factors were taken into consideration when comparing the combinations: system oversizing, crop requirement satisfaction, and investment cost.

2.1. Problem Statement

The review of the literature demonstrates the wide range of research initiatives aimed at improving the effectiveness and efficiency of water pumping systems that are integrated with HRES, especially wind and PV. Even with the tremendous advancements in this area, there are still a number of problems and gaps that need to be looked into further. The need for thorough and standard procedures to optimize the design, control, and functioning of hybrid PV-wind connected water pumping systems serves as the main problem statement for this literature review.

The absence of a sizing and configuration model that can be used everywhere, the unpredictability of changing solar and wind conditions, and the requirement for complex control schemes to optimize energy extraction while maintaining dependable water pumping are some of the difficulties. Furthermore, the lack of a standard benchmark for evaluating system performance and the influence of outside variables on various configurations call for a more comprehensive and

standardized approach. For the purpose of advancing the effective and sustainable hybrid renewable energy-based water pumping systems that serve a variety of applications and geographical areas, these challenges must be addressed.

3. Proposed methodology

The methodology for smart flow management in hybrid PV-wind connected water pumping systems that are being proposed concentrates on the combined application of an optimized control algorithm and Unified Power Flow Controller (UPFC) in conjunction with Fuzzy Q-Learning to tune a PID controller that controls the motor speed.

The identification and mitigation of PQ problems through the use of UPFC constitute the first part of the methodology. The Kookaburra Optimization Algorithm is used to improve the UPFC and guarantee an efficient and optimized operation. This algorithm helps determine the best parameters for the UPFC to take into account changing solar and wind energy input conditions in order to address PQ issues effectively.

Furthermore, the online tuning of the PID controller that controls the motor speed in the water pumping system is carried out using a Fuzzy Q-Learning technique. Adaptive PID parameter tuning is made easier by the fuzzy Q-Learning algorithm, which takes into account system dynamics and real-time feedback. This contributes to the overall effectiveness and dependability of the water pumping system by ensuring optimal motor speed control in response to shifting environmental factors and energy availability.

The incorporation of Fuzzy Q-Learning gives the PID controller a learning mechanism that allows it to continuously adjust and optimize its parameters, improving the stability and response of the system. The proposed workflow is shown in Figure 1.

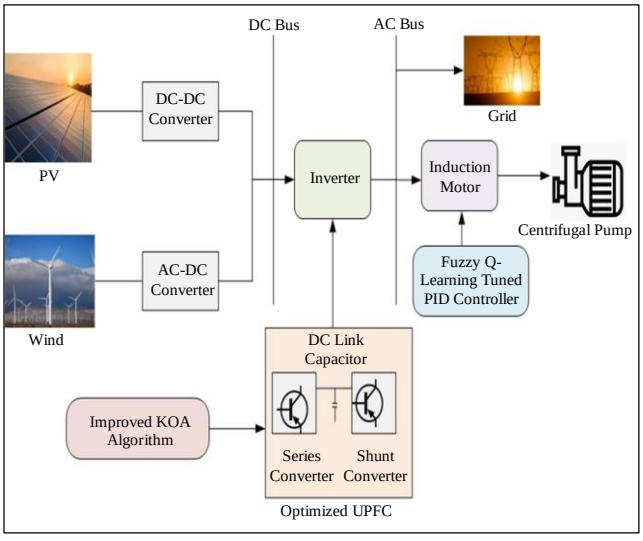

Fig. 1 The proposed water pumping system using hybrid PV-wind

3.1. Modelling of PV

The photovoltaic system uses sunlight to generate electricity directly, protecting the environment from harm. PV cells, which are merely basic p-n junction devices, make up the fundamental component of a PV array. A photocurrent serves as the current source, a diode connected in parallel to it, a resistor set in series to indicate the circuit's internal resistance to current flow, and a shunt resistance to represent leakage current make up an equivalent circuit. The amount of current applied to the load is expressed as,

$$I = I_{pv} - I_0\left[exp\left[\frac{V+IR_s}{aV_T}\right] - 1\right] - \left[\frac{V+IR_s}{R_p}\right]$$

Where a is the ideality factor, V is the voltage across the diode, I_0 is the reverse saturation current, and I_{pv} is the photocurrent current. Thermal voltage is denoted as V_T. Resistance in series and shunt are represented by R_s and R_p.PV cell photocurrent can be expressed as follows, depending on temperature and radiation.

$$I_{pv} = (I_{pv_{STC}} + K_I\Delta T)\frac{G}{G_{STC}}$$

The temperature coefficient of cell short circuit current is K_I. G_{STC}(W/m^2) stands for nominal solar irradiation, $I_{pv_{STC}}$ for current generated by light under typical test circumstances, and G stands for solar irradiation in W/m^2. The PV modelling is shown in Figure 2.

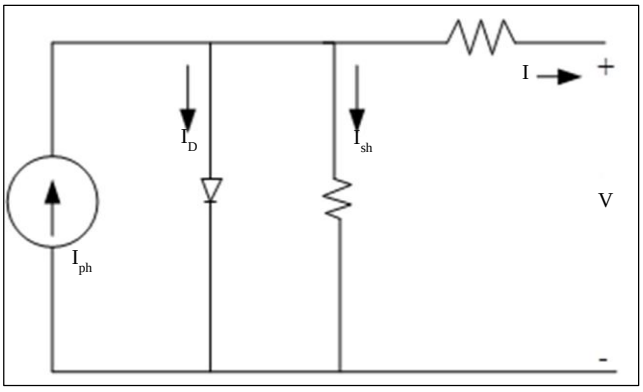

Fig. 2 PV modelling

3.2. Modelling of Wind

A wind turbine is a machine that converts air energy, or wind power, into mechanical power or the turbine's rotating motion. This mechanical power can then be used to power a generator or other device. The wind turbine blade's shape, pitch angle, rotational speed, and rotor radius all contribute to the power it captures. The power-generated equation is displayed below.

$$P_M = \frac{1}{2}\pi\rho C_p(\lambda,\beta)R^2V^3$$

Where wind turbine power capture is represented as $P_M$the radius of the blade (in meters) and wind speed, expressed in meters per second are indicated as R and V. Pich angle is denoted as β in degrees and air density is expressed as ρ.

The tip-speed ratio, denoted by λ and is given as,

$$\lambda = \frac{\Omega R}{V}$$

Where Ωexpress the rotational speed of the rotor (in rad/sec).C_p can be represented as the tip-speed ratio function.

$$C_p = \frac{1}{2}\left(\frac{116}{\lambda_1} - 0.4\beta - 5\right) exp^{\frac{-16.5}{\lambda_1}}$$

$$\lambda_1 = \left(\frac{1}{\frac{1}{\lambda+0.089} - \frac{0.035}{\beta^3+1}}\right)$$

Where C_p is the wind turbine's power coefficient,λ_1 is the constant, andλ is the tip speed ratio.

3.3. Modelling of Induction Motor

An induction motor is modelled using the three-phase equation model; in this instance, the large number of equations to solve will result in a longer simulation time. As a result, the mathematical model of an induction machine in the dq axis employs Park's transformation, a method for transforming the induction motor's three-phase variables into two-phase dq reference parameters.

The induction motor's electrical modelling in the dq reference frame can be obtained by selecting the stator voltage ($V_{ds,}V_{qs}$), stator currents ($I_{ds,}I_{qs}$), rotor speed (ωR), and rotor flux ($\lambda_{dR,}\lambda_{qR}$) as state variables.

$$\frac{dI_{ds}}{dt} = \frac{1}{L_{stator}K_L}[-I_{ds}R_{ms} + KL_{stator}\omega_S.I_{qs} + \left(\frac{M}{L_R}\right)\left(\frac{\lambda_{dR}}{T_R}\right) + \omega_R\lambda_{qR} + V_{ds}$$

$$\frac{dI_{qs}}{dt} = \frac{1}{L_{stator}K_L}[-I_{qs}R_{ms} - KL_{stator}\omega_S.I_{ds} + \left(\frac{M}{L_R}\right)\left(\frac{\lambda_{dR}}{T_R}\right) - \omega_R\lambda_{qR} + V_{qs}$$

$$\begin{cases} \frac{d\lambda_{dR}}{dt} = \left(\frac{M}{T_R}\right)I_{ds} + (\omega_S - \omega_R)\lambda_{qR} - \left(\frac{\lambda_{dR}}{T_R}\right) \\ \frac{d\lambda_{qR}}{dt} = \left(\frac{M}{T_R}\right)I_{qs} - (\omega_S - \omega_R)\lambda_{qR} - \left(\frac{\lambda_{dR}}{T_R}\right) \\ R_{ms} = R_{stator} + \frac{R_{rotor}M^2}{L_R^2} \end{cases}$$

3.4. Unified Power Flow Controller

FACT devices are used to treat issues with system quality, improve system equilibrium, and achieve reliability. Since the UPFC has both series and shunt active power filters, it was selected from among the FACTS devices because of its wider effect on the system's quality and balance. The PID controller was utilized to regulate the UPFC, striving to achieve optimal values through the utilization of the KOA algorithm to optimize its regulation.

The controller controls the UPFC's performance by monitoring the system voltage in the event of a malfunction and then generating pulses to drive the two UPFC converters. This produces signals that raise the measured reference voltage and, in turn, lower system quality issues. Two controllers are present in the UPFC system, one for the shunt component and one for the series component, and it is illustrated in Figure 3.

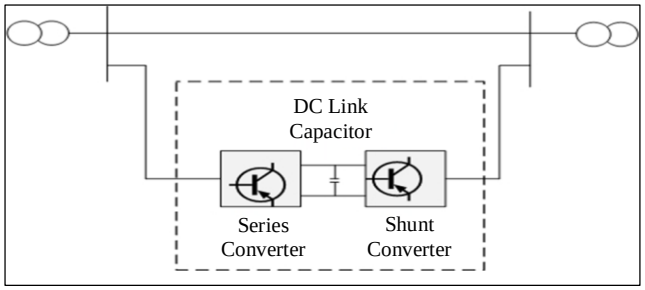

Fig. 3 Structure of UPFC

3.3.1. Control of Series Power Filter

Phase Locked Loop (PLL) is employed to calculate the three-phase voltage; the dq transformation (Clark transform) is used to convert it to d–q axes, as shown in Equation (2), Figure 4 depicts the series converter control of UPFC.

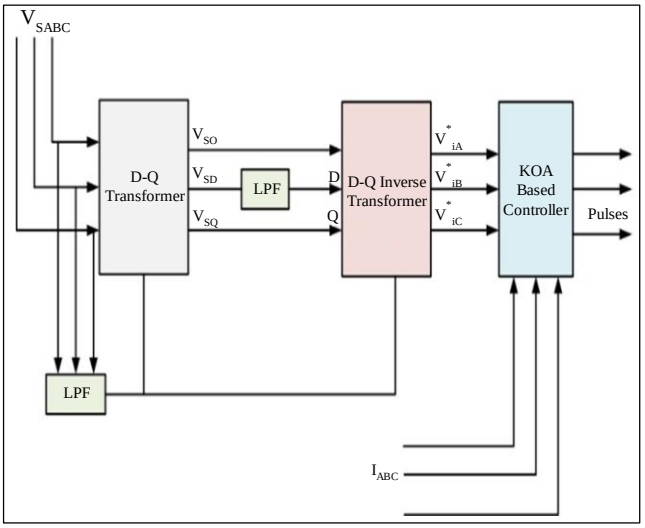

Fig. 4 Series converter control

$$\begin{bmatrix} V^0 \\ V^d \\ V^q \end{bmatrix} = \frac{2}{3}\begin{bmatrix} \frac{1}{2} & \frac{1}{2} & \frac{1}{2} \\ \sin(\alpha t) & \sin(\alpha t - \frac{2\pi}{3}) & \sin(\alpha t + \frac{2\pi}{3}) \\ \cos(\alpha t) & \cos(\alpha t - \frac{2\pi}{3}) & \cos(\alpha t + \frac{2\pi}{3}) \end{bmatrix}\begin{bmatrix} V^a \\ V^b \\ V^c \end{bmatrix}$$

Where V^a, V^b and V^c denotes the three-phase voltage and V^q is the quadrature axis voltage, The direct axis voltage, or V^d, can be used to smooth out both direct and alternating elements using an LPF as shown in Equation (3).

$$V^{d(dc)} = V^d - V^{d(ac)}$$

After that, the voltage dq is converted back to the three-phase voltage that Equation (4) uses as a reference voltage. As a result, before the filter is installed, the reference voltage and the system's inverter output can be compared. The PID controller then adjusts the difference signal via the KOA until it attains the reference value.

$$\begin{bmatrix} V^{Ra} \\ V^{Rb} \\ V^{Rc} \end{bmatrix} = \frac{2}{3}\begin{bmatrix} \sin(\alpha t) & \frac{1}{2} & 1 \\ \sin(\alpha t) & \sin(\alpha t - \frac{2\pi}{3}) & 1 \\ \cos(\alpha t) & \cos(\alpha t - \frac{2\pi}{3}) & 1 \end{bmatrix}\begin{bmatrix} V^{d(dc)} \\ V^q \\ V^0 \end{bmatrix}$$

3.3.2. Control of Shunt Power Filter

The control system starts by converting the voltage and current, α, β as indicated by Equation (5). The measured values of reactive power Q and active power P are then displayed in Equation (6). Shunt power control is illustrated in Figure 5.

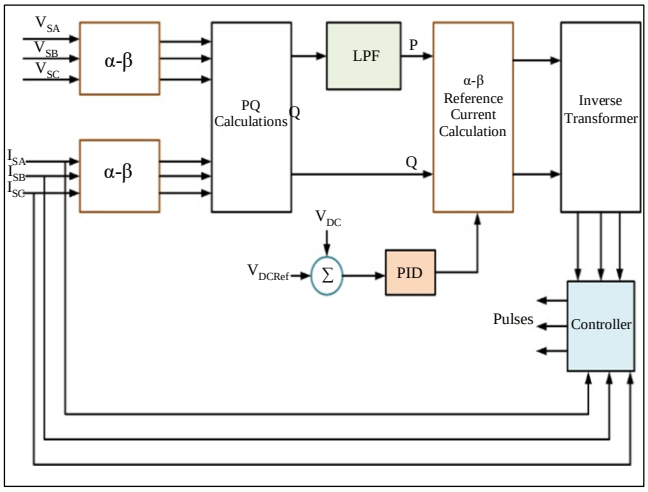

Fig. 5 Shunt converter control

$$\begin{bmatrix} I^0 \\ I^\alpha \\ I^\beta \end{bmatrix} = \sqrt{\frac{2}{3}}\begin{bmatrix} \frac{1}{\sqrt{2}} & \frac{1}{\sqrt{2}} & \frac{1}{\sqrt{2}} \\ 1 & -\frac{1}{2} & -\frac{1}{2} \\ 0 & \frac{\sqrt{3}}{2} & \frac{\sqrt{3}}{2} \end{bmatrix}\begin{bmatrix} I^a \\ I^b \\ I^c \end{bmatrix}$$

$$\begin{bmatrix} P \\ Q \end{bmatrix} = \begin{bmatrix} V^{s\alpha} & V^{s\beta} \\ -V^{s\beta} & V^{s\alpha} \end{bmatrix}\begin{bmatrix} I^\alpha \\ I^\beta \end{bmatrix}$$

The P is converted back into three-phase voltages, as shown in Equation (7), after passing over the LPF to measure the reference values for the α and β components. The measured voltages serve as the reference values that the KOA utilizes to contrast the source streams with the reference to calculate the PID parameter values necessary to generate the pulses that counter the error.

$$\begin{bmatrix} I^{Ra} \\ I^{Rb} \\ I^{Rc} \end{bmatrix} = \sqrt{\frac{2}{3}}\begin{bmatrix} 1 & 0 \\ -\frac{1}{2} & \frac{\sqrt{3}}{2} \\ -\frac{1}{2} & -\frac{\sqrt{3}}{2} \end{bmatrix}\begin{bmatrix} I^{R\alpha} \\ I^{R\beta} \end{bmatrix}$$

3.4. Kookaburra Optimization Algorithm

Since the kookaburras are arranged in the problem-solving space so that each one selects values for its decision variables according to where it is located, every member of the KOA population represents a potential vector solution to the problem. Equation (1) allows for the modelling of the KOA population matrix, which is composed of kookaburras. Equation (2) is used to randomly initialize the kookaburras' positions at the start of KOA implementation.

$$X = \begin{bmatrix} X_1 \\ \vdots \\ X_i \\ \vdots \\ X_N \end{bmatrix}_{N\times M} = \begin{bmatrix} x_{1,1} & \cdots & x_{1,d} & \cdots & x_{1,m} \\ \vdots & \ddots & \vdots & \iddots & \vdots \\ x_{i,1} & \cdots & x_{i,d} & \cdots & x_{i,m} \\ \vdots & \iddots & \vdots & \ddots & \vdots \\ x_{N,1} & \cdots & x_{N,d} & \cdots & x_{N,m} \end{bmatrix}_{N\times m}$$

$$x_{i,d} = lb_d + r.(ub_d - lb_d)$$

Here, N is the number of kookaburras,X is the KOA population matrix, r is a random number in the interval [0, 1],$x_{i,d}$ is its d^{th} dimension in search space,X_i is the ith kookaburra (candidate solution), m is the number of decision variables lb_d and ub_d are the lower and upper bounds of the decision variable, correspondingly.

Every kookaburra's location in the problem-solving space symbolizes a possible solution for any issue that corresponds to it, and this helps determine the problem's objective function. Equation (3) allows for the vector representation of the set of evaluated values for the problem's objective function. By iteratively updating the positions of kookaburras, which represent potential solutions in the PID parameter space, the KOA is used to search for the ideal PID parameters.

$$F = \begin{bmatrix} F_1 \\ \vdots \\ F_i \\ \vdots \\ F_N \end{bmatrix}_{N\times 1} = \begin{bmatrix} F(X_1) \\ \vdots \\ F(X_i) \\ \vdots \\ F(X_N) \end{bmatrix}_{N\times 1}$$

The evaluated objective function in this case is based on the i^{th} kookaburra, and its vector is denoted by F_i.

The KOA analysis iteratively upgrades the locations of kookaburras in the two stages of exploration and exploitation

to improve possible outcomes according to the simulation of actual kookaburra behaviours.

3.4.1. Hunting Strategy (Exploration)

The kookaburra is a carnivorous bird that consumes mice, frogs, insects, reptiles, and other small birds. Despite having weak legs, this bird's powerful neck aids in its ability to hunt. The way kookaburras choose and attack their prey causes them to move significantly in position. In this process, the global search is symbolized by the concept of exploration, which refers to the careful skimming of the problem-solving space to avoid getting trapped in the local optimal to locate the main optimal location.

To mimic the kookaburra hunting strategy, each kookaburra's position relative to other kookaburras whose objective function value is higher is taken into account when determining the prey location in the KOA design. Therefore, using the comparison of the objective function values, Equation (4) is utilized for determining the available prey set for each kookaburra.

$$CP_i = \{X_k : F_k < F_i \; and \; k \neq i\}$$

Where $i = 1,2,\ldots,N$ and $k \in \{1,2,\ldots.,N\}$

The kookaburra with a higher objective function than the i^{th} kookaburra is denoted by X_k the set of potential prey for ith kookaburra, and the objective function is represented by F_k . Each kookaburra is thought to choose its target at random and attack it according to the KOA design. Equation (5) is used to determine the kookaburra's new position based on the simulation of its movement towards the prey in the hunting strategy. In this instance, Equation (6) states that the new location will take the place of the respective kookaburra's previous position if the value of the objective function is enhanced there.

$$x_{i,d}^{P_1} = x_{i,d} + r.\left(SCP_{i,d} - I.x_{i,d}\right), i = 1,2,\ldots.,N \text{ and } d = 1,2,\ldots..,M$$

$$X_i = \begin{cases} X_i^{P_1}, F_i^{P_1} < F_i \\ X_i\,, \;\; else \end{cases}$$

In this case, $X_i^{P_1}$ is the newly proposed location of the ith kookaburra based on the first phase of KOA; $SCP_{i,d}$ is the d^{th} dimension of selected prey for i^{th} kookaburra, r is a random number with a normal distribution in the range of $[0,1]$, N is the number of kookaburra, $x_{i,d}^{P_1}$ is its d^{th} dimension; $F_i^{P_1}$ is its objective function value; I is a random number from set $\{1,2\}$; and m is the number of decision variables. The algorithm's global search can be carried out during the exploration phase, and local solution refinement occurs during the exploitation phase.

3.4.2. Ensuring that the Prey is Killed (Exploitation)

The second distinguishing behaviour of kookaburras is that, following an attack, they carry their prey with them and ensure that it is killed by repeatedly striking it against trees. After holding the prey firmly among its claws, the kookaburra squeezes and consumes it. Kookaburras exhibit this behaviour in close proximity to their hunting grounds, which causes slight shifts in their position. This procedure, which embodies the idea of exploitation in local search, speaks to the algorithm's capacity to produce better results close to areas of promise and already-obtained solutions.

Equation (7) is used to generate a random position in the KOA design, which simulates the kookaburra actions determined by movement close to the hunting area. Actually, it is presumed that this displacement happens at random in a neighborhood to each kookaburra's centre, with a radius equal to $\frac{(ub_d - lb_d)}{t}$. Initially, the neighborhood's radius is set to its maximum value. Subsequent iterations reduce this radius, allowing for a more precise local search that eventually converges to better solutions. If the objective function's value is improved by the new locations established for each kookaburra as per Equation (8), then it replaces the previous position.

$$x_{i,d}^{P_2} = x_{i,d} + (1 - 2r).\frac{(ub_d - lb_d)}{t} \; t = 1,2,\ldots.,T$$

$$X_i = \begin{cases} X_i^{P_2}, F_i^{P_2} < F_i \\ X_i\,, \;\; else \end{cases}$$

The updated position suggested for the kookaburra in considering the second KOA phase is denoted by $X_i^{P_2}$, where $x_{i,d}^{P_2}$ is its d^{th} dimension, $F_i^{P_2}$ is its objective function value, t is the algorithm's iteration counter, and T is the maximum number of algorithm iterations. In order to effectively explore the solution space and converge to the best PID parameters for the UPFC, the KOA seeks to strike a balance between exploration and exploitation by taking advantage of the traits of kookaburra hunting behavior.

To improve power system performance, the UPFC, PID controller, and kookaburra optimization algorithm work together to optimize the UPFC's control strategy. By fine-tuning the PID parameters, the KOA serves as an optimization tool that guarantees the UPFC performs at its best under a range of circumstances.

3.5. PID

A three-term controller is the PID controller. The PID controller regulates the plant input and its output is based on the error (e), which is the plant output less the set point (r) or reference signal. The goal of the PID control algorithm is to reduce error.

To improve system response speed and lower steady-state error, the proportional gain (K_P) is applied to cause the control signal $u(t)$ to react to the error right away. Although it eliminates the offset error, the integral gain (K_i) overshoots the system response. The derivative gain (K_d) is used to lessen the overshoot in the system response. Figure 6 shows the block diagram of a PID controller, and its transfer function is,

$$G_{PID} = K_P + K_i.\frac{1}{S} + K_d.s$$

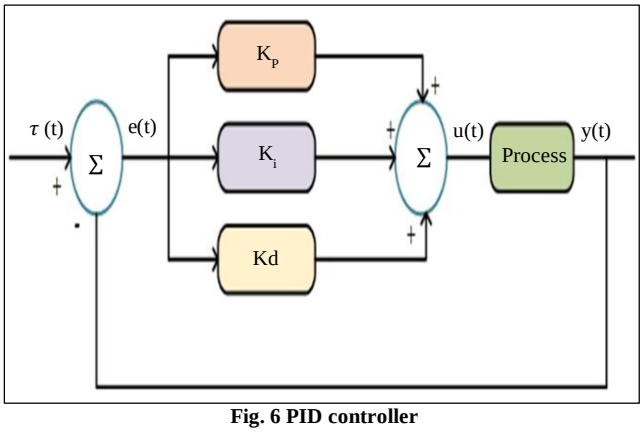

Fig. 6 PID controller

3.6. Fuzzy Q Learning for Online Tuning

Fuzzy Q-Learning is employed for online tuning of the PID controller responsible for motor speed regulation in the water pumping system. Adaptive PID parameter tuning is made easier by fuzzy Q-learning and is dependent on system dynamics and real-time feedback. The water pumping system's overall efficiency and dependability are enhanced by this dynamic tuning, which guarantees ideal motor speed control in the face of fluctuating energy availability and environmental conditions.

A mathematical system entirely reliant on digital logic is called a fuzzy control system. Fuzzification, membership function, rule-based formation, and defuzzification are the four stages in which the controlling procedure can be carried out in fuzzy logic. Fuzzification is the process of converting analog input into fuzzy sets and expressing the input and output graphically under the membership function (i.e., bell-shaped membership function). A rule-based formation can be used to express the relationship between the input and output. Fuzzy if/then rules are the primary benefit of fuzzy logic systems. These rules can use linguistic terms to express relations among fuzzy variables and embed expert knowledge. The fuzzy rule's general form is:

$$Ru: if\ (x_1\ is\ D_1)\ \ and/or\ (x_2\ is\ D_2)\ \ \ldots..and\ /\ or\ \ (x_m\ is\ D_m)\ \ then\ \ (c\ is\ E)$$

Where $D_j,\ j = 1, \ldots., m$ is an input fuzzy set of j, the crisp input vector is denoted by $x = (x_1, x_2, \ldots., x_m)$, the output variable is c, and the fuzzy set defined by the expert is represented by E. The conditions of the variable inputs that must be met in order for the firing strength $w_i(x)$of the rule to occur are combined by the operators "and/or."The Wang-Mendel model can be used to calculate the FLS's global output.

$$a(x) = \frac{\sum_{i=1}^{N} w_i(x) a_i}{\sum_{i=1}^{N} w_i(x)}$$

Where a_i is the outcome of i.

Every state-action pair in Q-Learning has its Q-values updated and stored. The implementation might not be feasible in situations where there are many state-action pairs. The benefit of using fuzzy inference systems is that they can produce accurate approximations in the Q-function while also enabling the application of fuzzy Q-learning to continuous states-space problems. The crisp set of inputs that define the agent's state in fuzzy Q-learning is denoted by x. These are transformed into fuzzy values, and a particular fuzzy rule represents every state.

Stated differently, the firing strength of each rule determines the degree to which an agent is in a state. Additionally, the rules lack fixed consequents, which means that instead of predefined, fixed state-action pairs, each rule's consequents (state-action pair) emerge from the exploration/exploitation algorithm. As a result, the FIS has opposing actions for every regulation, which take the following form:

$$\begin{array}{ll} if\ x\ is\ S_i & then\ \alpha[i,1] \\ & or\ \alpha[i,2] \\ & \vdots \\ & or\ \alpha[i,k] \end{array}$$

Where the k^{th} possible action in the rule i is represented by $\alpha[i,k]$, in rule i, there is a corresponding value $q[i,k]$ for every possible action. When the rule i is fired, this corresponding value establishes how "good" the corresponding action is. ($x_1 is S_{i,1} and x_2 is S_{i,2} \ldots and x_n is S_{i,n}$) defines the state S_i, where $S_{i,j}$, $j = 1, \ldots, n$ are fuzzy sets.In particular, the fuzzy Q-learning algorithm is briefly described below.

- Observe state x.
- Apply the exploration/exploitation algorithm to every rule i and take appropriate action α_i.
- Compute $a(x)$ as the global output using Equation (10).
- The corresponding value $Q(x,a)$ should be calculated using Equation (11).

$$Q(x,a) = \frac{\sum_{i=1}^{N} w_i(x) a_i\, q[i,i^+]}{\sum_{i=1}^{N} w_i(x)}$$

Where $q[i, i^+]$ is the matching q-value of the fired rule i for the exploration algorithm's choice of action i^+.

- Get the updated state data.
- Determine the reward $R(x, a, x')$.
- Adjust Q-values in accordance with Equation (12).

$$\Delta q[i, i^+] = \eta \Delta Q \frac{w_i(x)}{\sum_{i=1}^{N} w_i(x)}$$

$$\Delta Q = R(x, a, x') + \gamma . Q(x', a^*) - Q(x, a)$$

$$Q(x', a^*) = \frac{\sum_{i=1}^{N} w_i(x') a_i \, q[i, i^*]}{\sum_{i=1}^{N} w_i(x')}$$

$q[i, i^*]$ represents the choice of action i^* with the highest Q value for the fired rule i.

4. Result and Discussion

A thorough analysis of the effectiveness of the proposed approach in controlling power quality events is provided by the results and discussion that have been presented for the hybrid PV-wind connected water pumping system. The proposed system is implemented in MATLAB/Simulink. A variety of electrical parameters, including voltage, current, sag, swell, fluctuation mitigation, and Total Harmonic Distortion (THD), are included in the simulation.

The microgrid voltage, injected voltage, and compensated voltage are the various electrical parameters that are represented on the graph over time, as shown in Figure 7. These graphical representations allow for the visualisation and analysis of voltage distortions and their mitigation, as well as the unbalanced current resulting from the unbalanced load and compensated current in the grid system.

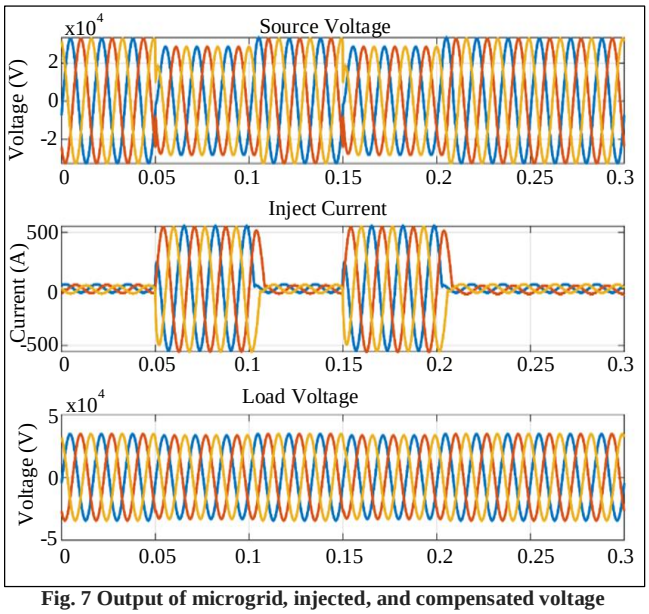

Fig. 7 Output of microgrid, injected, and compensated voltage

The injected current from the UPFC shunt converter is displayed under fundamental and third order frequencies in the first graph. The unbalanced load's effect on the unbalanced current is displayed in the second graph. The grid system's compensated current is displayed in the third graph. At the grid side, the compensated voltage is measured.

Oscillating lines in the microgrid voltage show periodic variations in injected currents at various frequencies or conditions. A similar pattern is seen in the injected voltage, although there are some noticeable variations or distortions in some of the line segments. Cleaner, more sinusoidal waves are seen in the compensated voltage, indicating that distortions have been lessened by the compensation mechanisms to produce a more balanced current flow.

The voltage, current, and compensated current are the various electrical parameters that are represented on the graph over time, as shown in Figure 8.

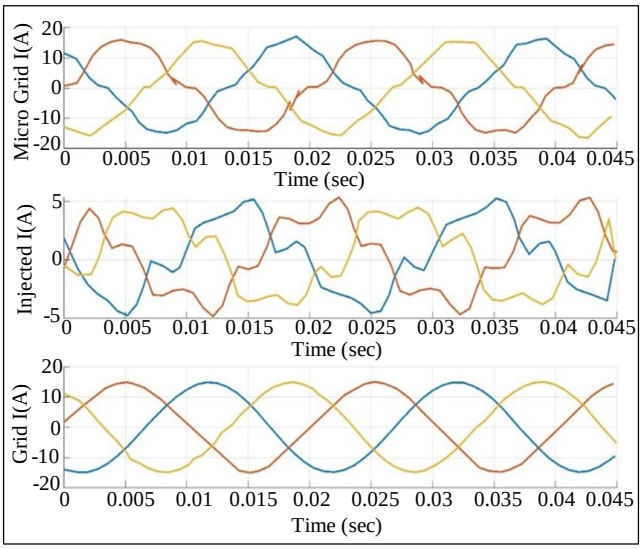

Fig. 8 Output of microgrid, injected and compensated current

The unbalanced current resulting from the unbalanced load is depicted in the first graph. The injected current from the UPFC shunt converter at fundamental and third order frequencies is depicted in the second graph. After employing a DPFC controller to reduce harmonic distortion brought on by nonlinear and unbalanced loads, the grid system's compensated current is shown in the figure.

The system under consideration is linked to both linear and unbalanced loads or distinct load conditions. Unbalanced conditions impact the microgrid current due to the use of nonlinear loads. The grid side measures the compensated current, and the UPFC's shunt converter aids in reducing unbalanced conditions. A UPFC controller was used to offset the harmonic distortion of the grid current caused by the unbalanced and nonlinear loads.

The analysis of voltage sag, swell, and fluctuation is paramount in assessing the effectiveness of a power system, especially in a grid-connected environment. The voltage quality analyses are essential for understanding the performance of the system when used in conjunction with the Unified Power Flow Controller (UPFC), Fuzzy Q-Learning, and optimized control algorithm for PID controller tuning in a hybrid PV-wind connected water pumping system.

4.1. Sag Analysis

The graphs representing electrical parameters over time, specifically source voltage, inject current, and load voltage for sag mitigation, are depicted in Figure 9.

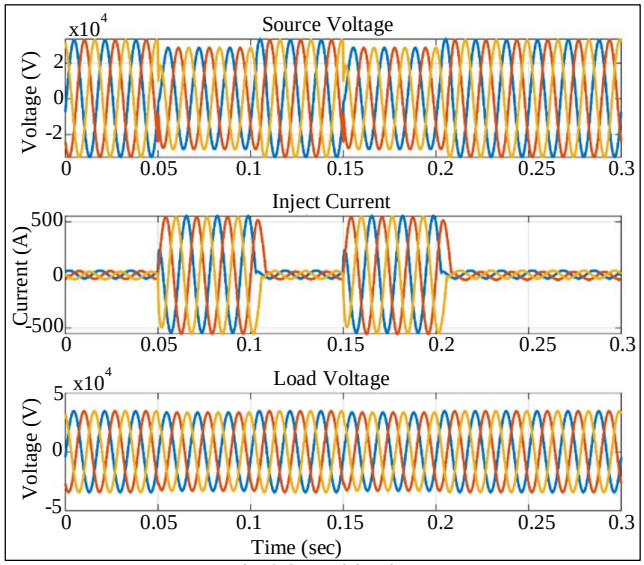

Fig. 9 Sag mitigation

Oscillating lines on the Source Voltage display show the voltage levels over time. Multiple lines indicate different phases or measurements. There is an approximate oscillation of $-2x10^4$ to $2x10^4$ V in the voltage. The inject current displays current levels that initially seem stable but then significantly decrease (sag) for about 0.15 seconds before rising again. There is an approximate oscillation in current between -500A and 500A. There is no discernible sag in the voltage levels over time, as indicated by the oscillating lines displayed by the load voltage. Between roughly $-5x10^4$ and $5x10^4$ V, the voltage oscillates.

4.2. Swell Analysis

Figure 10 depicts the voltage swell mitigation analysis. The graphs show the changes in electrical parameters over time, namely load voltage, inject current, and source voltage. The graphs help interpret the swell mitigation by showing how the voltage and current change over time. Oscillating lines on the Source Voltage display show the voltage levels over time. The injected current oscillates between -2000A and 2000A. Between roughly $-2x10^5$ and $2x10^5$ V is where the voltage oscillates.

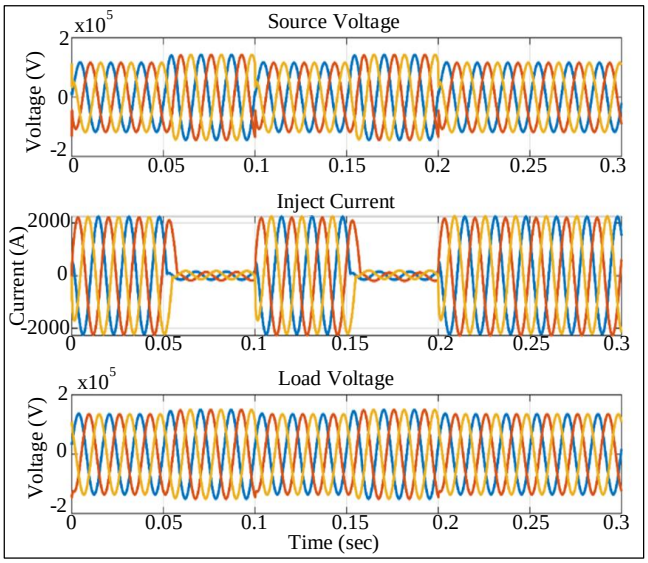

Fig. 10 Swell mitigation

4.3. Fluctuation Analysis

Figure 11 depicts the voltage fluctuation mitigation analysis. The source voltage varies from -1.98×10^5 to 1.98×10^5 V. The inject current varies from -2000 to 2000 A. The load voltage range varies from 1.98×10^5 to 1.98×10^5 V. In combination with the proposed approach, the thorough analyses of voltage sag, swell, and fluctuation offer strong proof of the system's robustness and its capacity to maintain steady and dependable operation under a variety of demanding grid conditions.

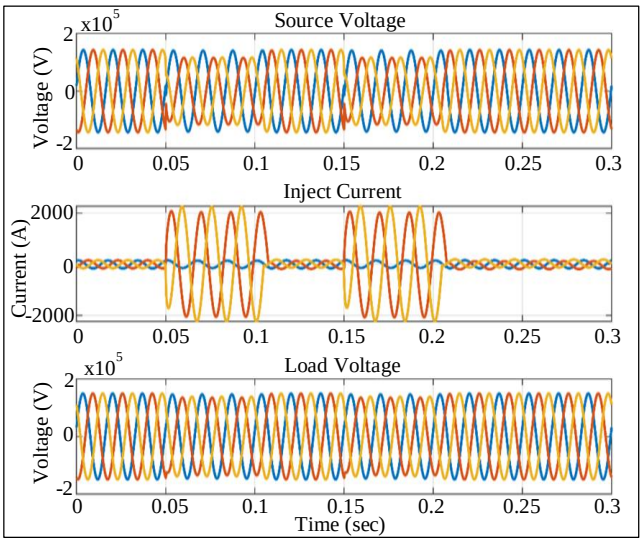

Fig. 11 Fluctuation mitigation

Figure 12 shows the comparison of the proposed and existing algorithms. The KOA (proposed) algorithm is used to control the injected voltages in order to adjust for the voltage output of the proposed system, improving the performance of the UPFC. The proposed algorithm is efficient compared to the other existing algorithms PSO, ABC and HBO.

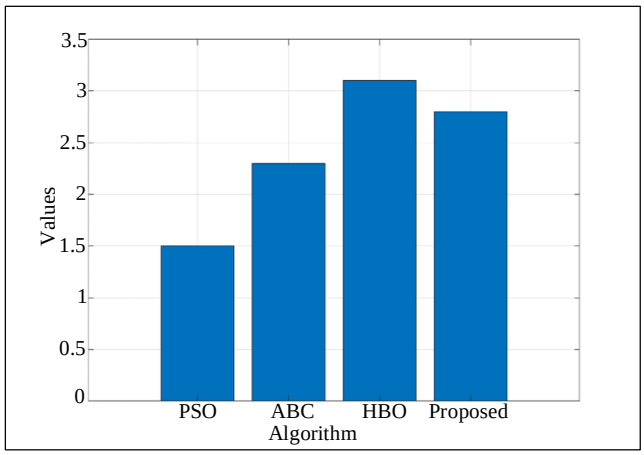

Fig. 12 Comparison of proposed and existing algorithm

4.4. THD Analysis

Figure 13 illustrates the THD analysis. THD is a percentage of the fundamental frequency, which is usually 50 or 60 Hz in grid power, and represents the total harmonic content in an electrical system. Unwanted electrical frequencies that arise as multiples of the fundamental frequency are known as harmonic distortions.

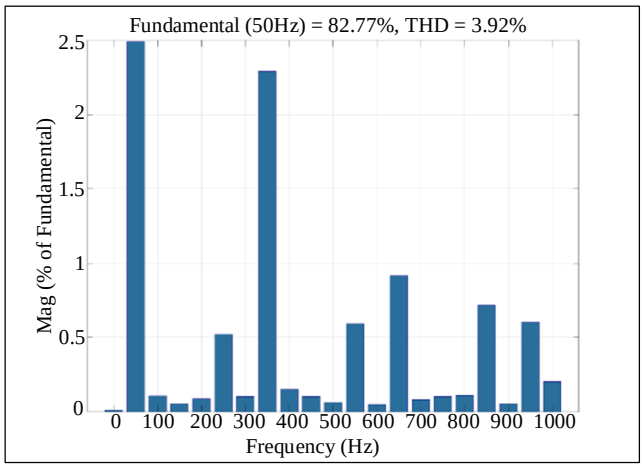

Fig. 13 THD analysis

These harmonics, which can arise from non-linear loads like power converters and electronics, can lower the voltage and current waveform quality of electrical power. The value of the THD is marked as 3.92 for 50Hz. This THD value, which accounts for 3.92 % of the total signal, indicates that there are harmonic components in the electrical system. The importance of THD in power quality assessment must be explained in order to put this result into perspective.

5. Conclusion

The integration of renewable energy sources into water pumping systems in remote areas is proposed as a comprehensive approach to improve their performance and reliability in this research. In particular, a novel methodology that combines an optimized control algorithm, UPFC, and fuzzy Q-learning for PID controller tuning is used to design a hybrid PV-wind connected water pumping system.

The study focuses on the identification and mitigation of PQ issues, effective power flow management, and PID controller optimization for motor speed control. System stability and reliability are enhanced by the UPFC, which is used to detect and address power quality issues. By optimizing UPFC parameters, the kookaburra optimization algorithm ensures effective and optimal performance under a range of solar and wind energy conditions. The PID controller that regulates motor speed is online tuned using fuzzy Q-learning, which offers adaptive parameter tuning based on system dynamics and real-time feedback.

The outcomes of the MATLAB/Simulink simulation show how well the proposed approach works to regulate power quality events. The robustness of the system is revealed by the thorough examinations of electrical parameters like voltage, current, sag, swell, fluctuation, and THD. Furthermore, by outperforming other algorithms like PSO, ABC, and HBO, KOA demonstrates its effectiveness in optimizing UPFC parameters.

The THD analysis highlights the system's capacity to maintain high-quality electrical waveforms by showing a low percentage of harmonic distortion. In future, the integration of energy storage devices, like batteries, can be examined to store extra energy produced when renewable resource availability is at its peak. This would improve the system's ability to deliver a steady and dependable water supply even when energy generation is low.

References

[1] Ali Mostafaeipour et al., "A New Model for the Use of Renewable Electricity to Reduce Carbon Dioxide Emissions," *Energy*, vol. 238, 2022. [CrossRef] [Google Scholar] [Publisher Link]

[2] Ashif Mohammad, and Farhana Mahjabeen, "Revolutionizing Solar Energy: The Impact of Artificial Intelligence on Photovoltaic Systems," *International Journal of Multidisciplinary Sciences and Arts*, vol. 2, no. 1, pp. 1-11, 2023. [Google Scholar] [Publisher Link]

[3] José-Ángel Garrido-Sarasol et al., "Technical Performance Analysis of High-Voltage Battery-Based Photovoltaic Water Pumping Systems," *Energy Conversion and Management: X*, vol. 22, pp. 1-21, 2024. [CrossRef] [Google Scholar] [Publisher Link]

[4] Sergio Gualteros, and Daniel R. Rousse, "Solar Water Pumping Systems: A Tool to Assist in Sizing and Optimization," *Solar Energy*, vol. 225, pp. 382-398, 2021. [CrossRef] [Google Scholar] [Publisher Link]

[5] Zafar A. Khan, "Assessment of Wind and Solar Hybrid Energy for Agricultural Applications in Sudan," *Energies*, vol. 15, no. 1, pp. 1-18, 2022. [CrossRef] [Google Scholar] [Publisher Link]

[6] António Couto, and Ana Estanqueiro, "Assessment of Wind and Solar PV Local Complementarity for the Hybridization of the Wind Power Plants Installed in Portugal," *Journal of Cleaner Production*, vol. 319, 2021. [CrossRef] [Google Scholar] [Publisher Link]

[7] Siamak Jamshidi, Kazem Pourhossein, and Meysam Asadi, "Size Estimation of Wind/Solar Hybrid Renewable Energy Systems without Detailed Wind and Irradiation Data: A Feasibility Study," *Energy Conversion and Management*, vol. 234, 2021. [CrossRef] [Google Scholar] [Publisher Link]

[8] Pradosh Kumar Sharma et al., "Energy Storage System Based on Hybrid Wind and Photovoltaic Technologies," *Measurement: Sensors*, vol. 30, 2023. [CrossRef] [Google Scholar] [Publisher Link]

[9] Jamiu Omotayo Oladigbolu, Makbul A.M. Ramli, and Yusuf A. Al-Turki, "Optimal Design of a Hybrid PV Solar/Micro-Hydro/Diesel/Battery Energy System for a Remote Rural Village under Tropical Climate Conditions," *Electronics*, vol. 9, no. 9, pp. 1-22, 2020. [CrossRef] [Google Scholar] [Publisher Link]

[10] Asma Charaabi et al., "A Novel Two Stage Controller for a DC-DC Boost Converter to Harvest Maximum Energy from the PV Power Generation," *Actuators*, vol. 9, no. 2, pp. 1-18, 2020. [CrossRef] [Google Scholar] [Publisher Link]

[11] Bahaa Saleh et al., "Performance Analysis of Maximum Power Point Tracking for Two Techniques with Direct Control of Photovoltaic Grid-Connected Systems," *Energy Sources, Part A: Recovery, Utilization, and Environmental Effects*, vol. 44, no. 1, pp. 413-434, 2022. [CrossRef] [Google Scholar] [Publisher Link]

[12] Julio López Seguel, S.I. Seleme, and Lenin M.F. Morais, "Comparison of the Performance of MPPT Methods Applied in Converters Buck and Buck-Boost for Autonomous Photovoltaic Systems," *INGENIARE-Revista Chilena de Ingeniería*, vol. 29, no. 2, pp. 229-244, 2021. [Google Scholar] [Publisher Link]

[13] G. Kannayeram, N.B. Prakash, and R. Muniraj, "Intelligent Hybrid Controller for Power Flow Management of PV/Battery/FC/SC System in Smart Grid Applications," *International Journal of Hydrogen Energy*, vol. 45, no. 41, pp. 21779-21795, 2020. [CrossRef] [Google Scholar] [Publisher Link]

[14] Hiba Nadhim A. Al-Kaoaz, and Ahmed Nasser B. Alsammak, "Performance Enhancement of Distance Relay in the Presence of a Unified Power Flow Controller," *International Journal of Power Electronics and Drive Systems (IJPEDS)*, vol. 14, no. 3, pp. 1577-1588, 2023. [CrossRef] [Google Scholar] [Publisher Link]

[15] Xiaomin Liu et al., "Suboptimal Control for Nonlinear Slow-Fast Coupled Systems Using Reinforcement Learning and Takagi-Sugeno Fuzzy Methods," *International Journal of Adaptive Control and Signal Processing*, vol. 35, no. 6, pp. 1017-1038, 2021. [CrossRef] [Google Scholar] [Publisher Link]

[16] Mohammad R. Altimania et al., "Optimal Performance of Photovoltaic-Powered Water Pumping System," *Mathematics*, vol. 11, no. 3, pp. 1-21, 2023. [CrossRef] [Google Scholar] [Publisher Link]

[17] J. M. Carricondo-Antón et al., "Optimization of an Isolated Photovoltaic Water Pumping System with Technical–Economic Criteria in a Water Users Association," *Irrigation Science*, vol. 41, pp. 817-834, 2023. [CrossRef] [Google Scholar] [Publisher Link]

[18] André de Oliveira Ferreira et al., "Modeling, Control and Simulation of a Small Photovoltaic-Wind Water Pumping System without a Battery Bank," *Computers & Electrical Engineering*, vol. 84, 2020. [CrossRef] [Google Scholar] [Publisher Link]

[19] Bader Alqahtani, Jin Yang, and Manosh C. Paul, "Design and Performance Assessment of a Pumped Hydropower Energy Storage Connected to a Hybrid System of Photovoltaics and Wind Turbines," *Energy Conversion and Management*, vol. 293, pp. 1-18, 2023. [CrossRef] [Google Scholar] [Publisher Link]

[20] Amine Ben Rhouma et al., "Improved Control Strategy for Water Pumping System Fed by Intermittent Renewable Source," *Energies*, vol. 16, no. 22, pp. 1-17, 2023. [CrossRef] [Google Scholar] [Publisher Link]

[21] Dan Li et al., "Sizing Optimization and Experimental Verification of a Hybrid Generation Water Pumping System in a Greenhouse," *Mathematical Problems in Engineering*, pp.1-11, 2020. [CrossRef] [Google Scholar] [Publisher Link]

[22] Hale Bakır, Adel Merabet, and and Mohammadali Kiehbadroudinezhad, "Optimized Control of a Hybrid Water Pumping System Integrated with Solar Photovoltaic and Battery Storage: Towards Sustainable and Green Water-Power Supply," *Energies*, vol. 16, no. 13, pp. 1-16, 2023. [CrossRef] [Google Scholar] [Publisher Link]

[23] Ahmed S. Menesy et al., "Optimal Configuration of a Hybrid Photovoltaic/Wind Turbine/Biomass/Hydro-Pumped Storage-Based Energy System Using a Heap-Based Optimization Algorithm," *Energies*, vol. 16, no. 9, pp. 1-26, 2023. [CrossRef] [Google Scholar] [Publisher Link]

[24] Neeraj Priyadarshi et al., "An Improved Hybrid PV-Wind Power System with MPPT for Water Pumping Applications," *International Transactions on Electrical Energy Systems*, vol. 30, no. 2, 2019. [CrossRef] [Google Scholar] [Publisher Link]

[25] Ludmil Stoyanov et al., "Multivariate Analysis of a Wind–PV-Based Water Pumping Hybrid System for Irrigation Purposes," *Energies*, vol. 14, no. 11, pp. 1-28, 2021. [CrossRef] [Google Scholar] [Publisher Link]